### Title

Engineering the Ratios of Nanoparticles Dispersed in Triphasic Nanocomposites for Biomedical Applications.




### Authors

Wetteland, Cheyann

Xu, Changlu

Wang, Sebo

et al.



### Publication Date

2025-01-06

### DOI

10.1021/acsami.4c14712

Peer reviewed

ACS APPLIED MATERIALS & INTERFACES



www.acsami.org
Research Article

# Engineering the Ratios of Nanoparticles Dispersed in Triphasic Nanocomposites for Biomedical Applications

Cheyann Wetteland, Changlu Xu, Sebo Michelle Wang, Chaoxing Zhang, Elizabeth Juntilla Ang, Cole Gabriel Azevedo, and Huinan Hannah Liu*

Cite This: ACS Appl. Mater. Interfaces 2025, 17, 3852−3865
Read Online



**ABSTRACT:** Polymer/ceramic nanocomposites integrated the advantages of both polymers and ceramics for a wide range of biomedical applications, such as bone tissue repair. Here, we reported triphasic poly(lactic-*co*-glycolic acid) (PLGA, LA/GA = 90:10) nanocomposites with improved dispersion of hydroxyapatite (HA) and magnesium oxide (MgO) nanoparticles using a process that integrated the benefits of ultrasonic energy and dual asymmetric centrifugal mixing. We characterized the microstructure and composition of the nanocomposites and evaluated the effects of the HA/MgO ratios on degradation behavior and cell−material interactions. The PLGA/HA/MgO nanocomposites were composed of 70 wt % PLGA and 30 wt % nanoparticles made of 20:10, 25:5, and 29:1% by weight of HA and MgO, respectively. The results showed that the nanocomposites had a homogeneous nanoparticle distribution and as-designed elemental composition. The cell study indicated that reducing the MgO content in the triphasic nanocomposite increased the BMSC adhesion density under both direct and indirect contact conditions. Specifically, after the 24 and 48 h of culture, the PLGA/HA/MgO group with a weight ratio of 70:29:1 (P70/H29/M1) exhibited the greatest average cell adhesion density under direct and indirect contact conditions among triphasic nanocomposites. During a 28-day degradation study, the mass loss of triphasic nanocomposites was 18 ± 2% for P70/H20/M10, 9 ± 2% for P70/H25/M5, and 7 ± 1% for P70/H29/M1, demonstrating that MgO nanoparticles accelerated the degradation of the nanocomposites. Postculture analysis showed that the pH values and $Mg^{2+}$ ion concentrations in the media increased with increasing MgO content in the nanocomposites. Triphasic nanocomposites provided different degradation profiles that can be tuned for different biomedical applications, especially when a shorter or longer period of degradation would be desirable for optimal bone tissue regeneration. The concentration and ratio of nanoparticles should be adjusted and optimized when other polymers with different degradation modes and rates are used in the nanocomposites.

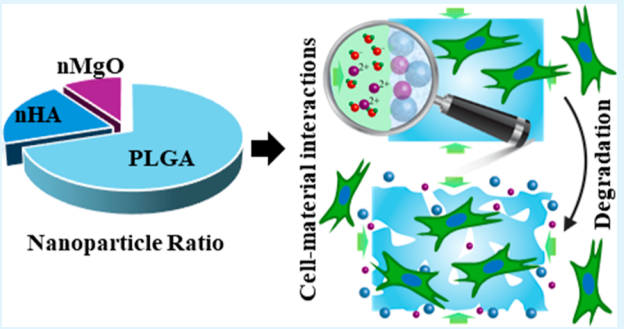


**KEYWORDS:** *magnesium oxide (MgO), hydroxyapatite (HA), poly(lactic-co-glycolic acid) (PLGA), triphasic nanocomposites, biodegradation, cell−material interactions, bone marrow-derived mesenchymal stem cells (BMSCs)*

## 1. INTRODUCTION

There is a growing clinical need for bone tissue regeneration in contemporary society with an aging population.[1] Autograft is considered as the "golden standard" for bone tissue repair since they are osteoinductive, osteoconductive, and nonimmunogenic.[2] However, limited supply, morbidity at the donor site, and long operating hours have severely hampered the use of autografts.[2,3] Allograft is another type of osteoinductive and osteoconductive material for bone regeneration, but their use has been restricted by high cost, high risk of disease transmission, and immunological rejection.[4−6] To address the aforementioned issues with autografts and allografts, biomaterials such as polymers,[7] ceramics,[8,9] metals,[10] and their composites[11,12] have been widely explored for bone regeneration.[13] For example, polymers such as poly(L-lactic acid) (PLLA)[7] and poly(lactic-*co*-glycolic acid) (PLGA)[14] have been extensively studied and used for orthopedic applications due to their excellent biocompatibility and biodegradability. Nevertheless, polymers typically have insufficient bioactivity and low mechanical strength. Ceramics such as hydroxyapatite (HA) have excellent bioactivity and relatively high mechanical strength, but it can take years for crystalline HA to fully degrade in the biological environment.[15] To maximize the efficacy for bone regeneration, it is highly desirable that biomaterials could resemble bone tissue functionally, structur-

Received: September 2, 2024
Revised: November 25, 2024
Accepted: November 27, 2024
Published: January 6, 2025

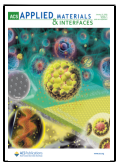

Table 1. Composition of Triphasic Nanocomposites of PLGA/HA/MgO and Subsequent Biphasic and Single-Phase Controls[a]

| | abbreviations | material components (mg) | | | component concentration in culture (mg/mL) | | | comments |
|---|---|---|---|---|---|---|---|---|
| | | PLGA | HA | MgO | PLGA | HA | MgO | |
| triphasic nanocomposites | P70/H20/M10 | 12 | 3.4 | 1.7 | 4 | 1.13 | 0.56 | 70% P, 20% H, and 10% M |
| | P70/H25/M5 | 11.6 | 4.2 | 0.8 | 3.86 | 1.4 | 0.26 | 70% P, 25% H, and 5% M |
| | P70/H29/M1 | 11.4 | 4.7 | 0.2 | 3.8 | 1.56 | 0.06 | 70% P, 29% H, and 1% M |
| biphasic nanocomposites | P70/H20 | 12 | 3.4 | 0 | 4 | 1.13 | 0 | P70/H20/M10-M10 |
| | | | | | | | | 77.78% P and 22.22% H |
| | P70/H25 | 11.6 | 4.2 | 0 | 3.86 | 1.4 | 0 | P70/H25/M5-M5 |
| | | | | | | | | 73.68% P and 26.32% H |
| | P70/H29 | 11.4 | 4.7 | 0 | 3.8 | 1.56 | 0 | P70/H29/M1-M1 |
| | | | | | | | | 70.07% P and 29.29% H |
| | P70/H30 | 11.3 | 4.9 | 0 | 3.76 | 1.63 | 0 | 70% P and 30% H |
| | P70/M30 | 11.5 | 0 | 4.9 | 3.83 | 0 | 1.63 | 70% P and 30% M |
| | P70/M10 | 12 | 0 | 1.7 | 4 | 0 | 0.56 | P70/H20/M10-H20 |
| | | | | | | | | 77.78% P and 22.22% M |
| | P70/M5 | 11.6 | 0 | 0.8 | 3.86 | 0 | 0.26 | P70/H25/M5-H25 |
| | | | | | | | | 93.33% P and 6.67% M |
| | P70/M1 | 11.4 | 0 | 0.2 | 3.8 | 0 | 0.06 | P70/H29/M1-H29 |
| | | | | | | | | 98.59% P and 1.41% M |
| | H20/M10 | 0 | 3.4 | 1.7 | 0 | 1.13 | 0.56 | P70/H20/M10-P70 |
| | H25/M5 | 0 | 4.2 | 0.8 | 0 | 1.4 | 0.26 | P70/H25/M5-P70 |
| | H29/M1 | 0 | 4.7 | 0.2 | 0 | 1.56 | 0.06 | P70/H29/M1-P70 |
| single-phase controls | P70 | 12 | 0 | 0 | 4 | 0 | 0 | P70/H20/M10-H20-M10 |
| | H20 | 0 | 3.4 | 0 | 0 | 1.13 | 0 | P70/H20/M10-P70-M10 |
| | H25 | 0 | 4.2 | 0 | 0 | 1.4 | 0 | P70/H25/M5-P70-M5 |
| | H29 | 0 | 4.7 | 0 | 0 | 1.56 | 0 | P70/H29/M1-P70-M1 |
| | H30 | 0 | 4.9 | 0 | 0 | 1.63 | 0 | P70/301-P70 |
| | M30 | 0 | 0 | 4.9 | 0 | 0 | 1.63 | P70/M30-P70 |
| | M10 | 0 | 0 | 1.7 | 0 | 0 | 0.56 | P70/H20/M10-P70-H20 |
| | M5 | 0 | 0 | 0.8 | 0 | 0 | 0.26 | P70/H25/M5-P70-H25 |
| | M1 | 0 | 0 | 0.2 | 0 | 0 | 0.06 | P70/H29/M1-P70-H29 |

[a]The amount of each component is listed as the mass in mg for a single 1 $cm^2$ scaffold. Compositions of triphasic nanocomposites and biphasic and single-phase controls and relationships between groups are shown in the "Comments" column. For example, the comment for P70/H20 is "P70/H20/M10-M10", which indicates that biphasic P70/H20 as a control for triphasic P70/H20/M10 is similar to it but 10% MgO (M10) is subtracted.

ally, and mechanically. Natural bone is a nanocomposite composed of nanostructured collagen as the polymer matrix and a variety of calcium phosphates as the ceramic phases. Similarly, polymer/ceramic nanocomposites incorporated the benefits of both soft polymers and hard ceramics, which have been extensively studied and employed in different biomedical applications.[16−18]

HA has been widely used in the polymeric phase for orthopedic applications since it is a well-established calcium phosphate phase similar to naturally occurring bone minerals. Nano-HA (nHA) is both osteoconductive and osteoinductive,[19−21] which is essential for bone tissue regeneration. Naturally occurring bone minerals contain a range of other components such as zinc and magnesium, which are crucial for biological activities.[22,23] As a result, dopants such as $Mg^{2+}$ are sometimes added to HA synthesis to produce minerals that are more comparable to those of natural bone. Preosteoclasts exposed to calcium magnesium phosphate exhibited higher cell adhesion density and higher expression of runt-related transcription factor 2 (RUNX2), osteopontin (OPN), and alkaline phosphatase (ALP) than HA alone.[24] Other evidence also supported the synergistic effects of $Mg^{2+}$ and $Ca^{2+}$ ions on increasing cell proliferation and osteogenic activity of bone-forming cells.[24,25]

Magnesium oxide nanoparticle (nMgO) is another type of ceramic that is attractive for its antimicrobial properties and biological benefits to bone-forming cells for bone regeneration.[26−30] In our previous study, we systematically investigated the concentration-dependent behaviors of bone marrow derived mesenchymal stem cells (BMSCs) toward nMgO.[30] Specifically, nMgO at the concentrations of 500−2000 μg/mL decreased the adhesion density of newly seeded BMSCs after 24 h of direct culture, and BMSC adhesion density in the nMgO group of 200 μg/mL was statistically greater than that of other nMgO groups. After 24, 48, and 72 h of direct exposure culture, nMgO enhanced the proliferation of BMSCs at low doses of 200 μg/mL, but decreased the cell proliferation at high doses of >300 μg/mL.[30] Previous studies have utilized nMgO in composites with biodegradable polymers such as PLLA and PLGA for bone regeneration applications.[18,27] Hickey et al. reported that osteoblasts cultured on PLLA/MgO composites exhibited an increase in adhesion density and proliferation in vitro.[27] It also has been shown that PLGA loaded with 30% of nMgO decreased cell viability.[18] As a result, it is necessary to optimize the concentrations of nMgO to benefit from its positive effects on cell proliferation while minimizing unfavorable consequences.



https://doi.org/10.1021/acsami.4c14712
ACS Appl. Mater. Interfaces 2025, 17, 3852−3865

The objectives of this article were to engineer the ratios of HA and MgO nanoparticles well-dispersed in triphasic PLGA/HA/MgO nanocomposites and to evaluate the potential synergistic effects of HA and MgO nanoparticles on degradation behavior and cell−material interactions of triphasic nanocomposites. PLGA, a copolymer of poly(lactic acid) (PLA) and poly(glycolic acid) (PGA), was utilized as the polymeric matrix for nanoparticle incorporation. PLGA is a well-known biodegradable polymeric material used for biomedical applications.[31,32] PLGA-based drug delivery implants, such as Zoladex implant for delivering luteinizing hormone-releasing hormone agonist for treating hormone receptor-positive breast cancer and prostate cancer, have been approved by the US Food and Drug Administration.[33,34] Although PLGA nanocomposites incorporating HA or MgO nanoparticles have been widely developed, systematic studies on the composition-microstructure−property relationships of triphasic PLGA/HA/MgO nanocomposites are currently limited. Moreover, the dispersion of nanoparticles has a significant impact on the performance of nanocomposites for biomedical applications, which was mostly overlooked in previous studies. We systematically investigated the effects of composition and nanoparticle dispersion on the cell−material interactions and biodegradation behavior of PLGA/HA/MgO triphasic nanocomposites in this study and elucidated the composition-microstructure−property relationships for engineering triphasic polymer/ceramic nanocomposites toward different biomedical applications such as bone repair.

## 2. MATERIALS AND METHODS

**2.1. Preparation of MgO.** MgO nanoparticles were purchased from US Research Nanomaterials Inc. (US3310, 99+% purity, 20 nm diameter). MgO nanoparticles were sterilized in a glass container via heating at 200 °C in an oven for 1 h, prior to use in nanocomposites and exposure to physiologically relevant fluids.

**2.2. Preparation of HA.** HA was synthesized through wet precipitation as previously published.[18,35,36] Briefly, 1 M $Ca(NO_3)_2$ was added dropwise to 0.6 M $(NH_4)_2HPO_4$ at 40 °C at a rate of 30 drops per minute. This mixture underwent stirring for 20 h for reaction and precipitation of particles. The resulting particle and solution mixture were centrifuged at 3000 rpm for 1 min. The supernatant was discarded, and the particles were resuspended in deionized (DI) water. The centrifuging and resuspension in DI water were repeated 3 times to remove excess ammonia. After washing, the pellet was resuspended in DI water and transferred to an acid digestion bomb for hydrothermal treatment at 200 °C for 20 h. The suspension was then collected and centrifuged, followed by removal of the supernatant. The resulting particles were dried under vacuum at 80 °C for 12 h and then ground using a mortar and pestle. Prior to use in the preparation of composites or cell culture, the nHA was disinfected by heating in an oven at 200 °C for 1 h.

**2.3. Nanocomposites.** *2.3.1. Synthesis.* Composites were synthesized via mechanical dispersion and solvent casting as previously described.[18] PLGA/HA/MgO composites maintained a weight ratio of 7:3 for polymer/nanoparticles. The 30% nanoparticles were split between HA and MgO as 20:10, 25:5, and 29:1 and compared with biphasic nanocomposites of PLGA/MgO and PLGA/HA where each nanoparticle represented the whole 30%. Controls were developed for each triphasic composite. The amount of each component present in a scaffold is detailed in Table 1.

In a 20 mL vial, 0.443 g of PLGA (90:10 LA: GA, MW 125 kDa, AP49, Polyscitech) was added to 3.5 mL of chloroform ($CHCl_3$, Fisher Scientific). The resulting solution was sonicated in a low-power ultrasonic bath (Symphony, VWR) at 40 °C for 1 h to fully dissolve the polymer. HA was then added to the solution and incorporated by vortexing for 1 min, followed by speed mixing [dual asymmetric centrifugal (DAC) 150.1 FVZ-K, FlackTek, Inc.] at 2500 rpm for 5 min. The suspension then underwent high-powered probe sonication (Qsonica, Q125) for 10 min, with pulses of 5 s on and 5 s off. The suspension underwent a total of 3 cycles of high-powered sonication and speed mixing, ending with speed mixing at 3500 rpm for 5 min to improve the dispersion and remove bubbles. The suspension was then poured into an 8.3 cm by 4 cm Teflon dish, where the chloroform was allowed to evaporate in the air for 24 h. The nanocomposite was then placed back into a 20 mL vial, and 4 mL of chloroform was added. Low-powered sonication, speed mixing, and high-powered sonication were performed using the same cycles as the previous day. The suspension was then poured into a Teflon dish where chloroform was allowed to evaporate for 24 h in ambient conditions, followed by an additional 48 h of evaporation under vacuum. All biphasic controls, including PLGA/HA, were synthesized by using this same protocol. However, PLGA/MgO with 70:30 wt %, utilized 4.5 mL of chloroform for the first round of suspension and 4 mL of chloroform during the second round of suspension. This was necessary for samples with 30% MgO because of the interactions of MgO with polyesters that increased viscosity.[37]

The resulting scaffolds were cut into 10 mm × 10 mm squares with a thickness of 0.1 mm to be used in cell studies. Each scaffold was disinfected by soaking in 100% ethanol for 24 h before cell culture and degradation studies.

*2.3.2. Characterization.* A representative scaffold from each group was characterized via scanning electron microscopy (SEM, Philips XL30) to evaluate surface topography and attached energy-dispersive X-ray spectrometry (EDS, EDAX Leap detector) to confirm elemental composition. In preparation for SEM/EDS analysis, each composite was adhered to an aluminum SEM pin mount with copper tape. The mounted samples were then coated with platinum and palladium (Pt/Pd) by using a sputter-coater (108 Auto, Cressington). All SEM images were taken using a secondary electron detector at an accelerating voltage of 2 kV, a spot size of 3, a working distance of 10 mm, and a magnification of 10,000×. EDS was performed on the entire image area under the same conditions except the accelerating voltage was raised to 10 kV.

**2.4. BMSC Culture.** *2.4.1. Cell Culture.* BMSCs were extracted from the femur and tibia of Sprague−Dawley rat weanlings according to previously established protocols, approved by the Institutional Animal Care and Use Committee at the University of California at Riverside.[30,35,36,38] BMSCs were cultured in Dulbecco's Modified Eagle's Medium (DMEM) with 10% fetal bovine serum and 1% penicillin/streptomycin (P/S) by volume, herein referred to as just DMEM. BMSCs were cultured in standard cell culture conditions at 37 °C with 5% $CO_2$/95% air in a humidified environment (MCO-19AIC, Sanyo Scientific). BMSCs at their second passage were cultured to 90% confluency for use in cell experiments.

*2.4.2. Culture on Nanocomposites.* Nanocomposites were placed in wells of 12-well tissue culture treated plates (TCTP, Corning, Falcon 353043). Each composite was placed into its respective well and then rinsed with 2 mL of phosphate-buffered saline. Then 1 mL of DMEM was added to each composite well. The mass of the nanoparticles and the resulting concentration for bare nanoparticles are shown in Table 1. The nanoparticle controls were suspended via pipetting in 1 mL of DMEM and transferred to their respective wells. BMSCs at the second passage were seeded at a density of 10,000 cells/cm$^2$ directly onto the disinfected scaffolds in 2 mL of DMEM, bringing the total media volume in each well to 3 mL. The cells were cultured with scaffolds and controls for 24 h. Certain groups of nanocomposites and controls were eliminated from further culture for 48 h, if their cell density decreased after the 24-h culture. The remaining groups were cultured for 48 h. Media was exchanged every 24 h. At the end of each respective time point of 24 or 48 h, media was collected for further analysis. At the end of the prescribed 24 or 48 h of culture, BMSCs were fixed with 4% paraformaldehyde in PBS and stained with 4′,6-diamidino-2-Phenylindole, dihydrochloride (DAPI, Life Technologies), and Alexa Fluor 488 phalloidin (Life Technologies) to image the nuclei and cytoskeleton, respectively. BMSCs were imaged under a fluorescence microscope (Nikon Eclipse


https://doi.org/10.1021/acsami.4c14712
ACS Appl. Mater. Interfaces 2025, 17, 3852−3865

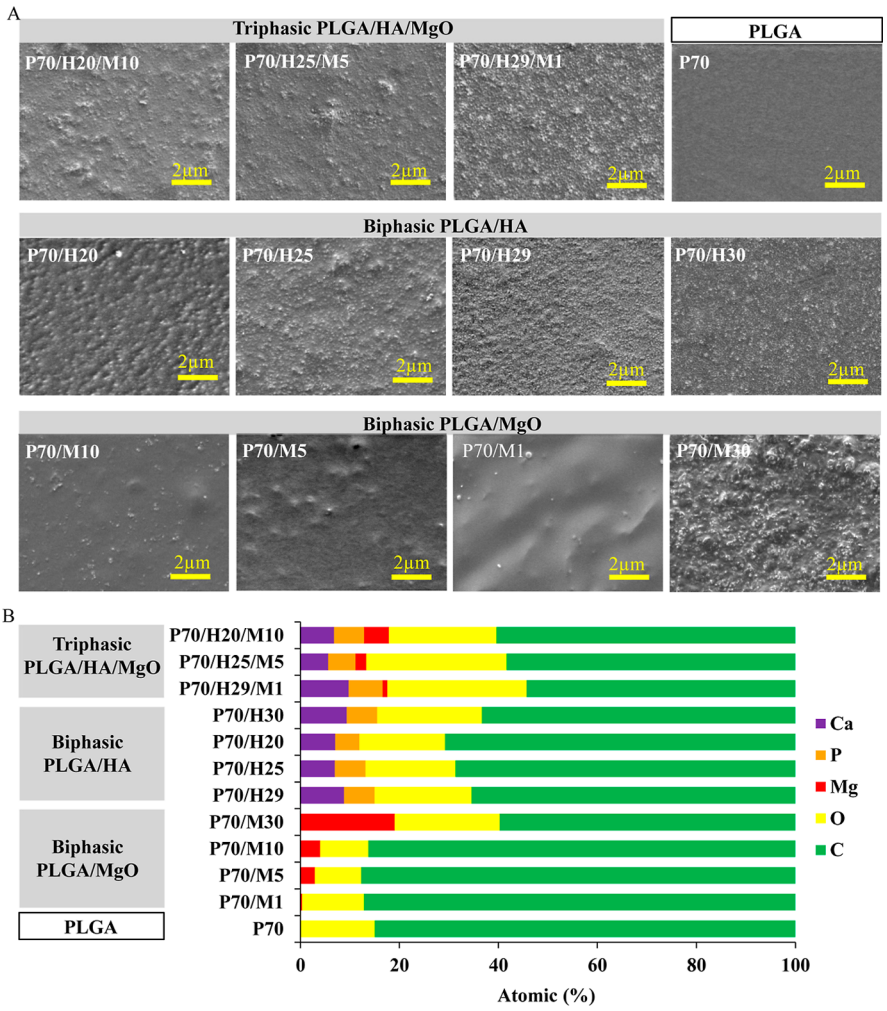


**Figure 1.** Microstructure and elemental composition of triphasic and biphasic nanocomposites and controls. (A) SEM micrographs showing the top surface of triphasic PLGA/HA/MgO, biphasic PLGA/HA and PLGA/MgO, and PLGA controls, at the original magnification of 10,000×. (B) Atomic percent of elements in the triphasic and biphasic nanocomposites and PLGA control as quantified by EDS analyses on the image areas for each corresponding sample in (A).

Ti), and 10 images were collected for each well. The fluorescence images of two stains were merged, and the cells were counted using the quantitative analysis tools in ImageJ. Then cell density was calculated as adherent cells per unit area.

*2.4.3. Postculture Media Analysis.* Immediately after collection, the pH of the media was determined using a benchtop pH meter (Symphony SB70P, VWR) to limit the effects of atmospheric $CO_2$ on the bicarbonate buffering system present in DMEM. Each media sample was then diluted 1:100 in DI water to prepare for analysis via induced coupled plasma−optical emission spectrometry (ICP-OES, Optima 8000, PerkinElmer). ICP-OES analysis was used to obtain media concentrations of $Mg^{2+}$ and $Ca^{2+}$ to evaluate the release of ions from the composites. Solutions of $Mg^{2+}$ and $Ca^{2+}$ at concentrations of 0.5, 1, and 5 ppm in nitric acid were used to generate a standard curve for all $Mg^{2+}$ and $Ca^{2+}$ measurements, respectively. Measurements were recorded as milligrams per liter for Mg and micrograms ($\mu$g) per liter for Ca. These values were then converted to mM by dividing by the molecular weight of Mg (24.305 g/mol) and Ca (40.078 g/mol) for each and dividing by 1000 in the case of Ca converting $\mu$M to mM.

**2.5. Degradation Study.** *2.5.1. Sterilization of Nanocomposites.* To mimic cellular conditions, the composites were disinfected in 100% ethanol as previously described in preparation for the degradation study.

*2.5.2. Degradation in DMEM.* Samples were placed in wells of 12 well plates and rinsed with PBS, as described for the cell study. Then, 3 mL of complete DMEM was added to each well and samples were placed in the incubator for 24 h, 48 h, 72 h, 5 days, 7 days, 14 days, and 28 days. At each time point, media was collected, and samples were rinsed in PBS and then allowed to dry. The dry postculture weight was measured at each time point, and the media underwent pH measurements and ICP-OES analysis.

*2.5.3. Post Degradation Mass Change.* Mass loss was calculated as a percentage of $(M_i - M_f)/M_i \times 100\%$, where $M_i$ was the initial mass and $M_f$ was the mass of the composite at its respective time points.

*2.5.4. Post Degradation Media Analysis.* The media from the acellular degradation study underwent the same analysis as that described in the cell culture. The pH was measured soon after collection to minimize the effects of atmospheric $CO_2$ and temperature. The media was then diluted 1:100 in DI water for ICP-OES analysis, which was used to measure free $Mg^{2+}$ and $Ca^{2+}$ ions.

**2.6. Statistical Analysis.** All experiments were run in triplicate. All data sets were analyzed using one-way analysis of variance, followed by the Tukey honest significant difference (HSD) post hoc test. Statistical significance was considered at $p < 0.05$.

## 3. RESULTS AND DISCUSSION

**3.1. Microstructure and Composition of Nanocomposites.** As shown in Figure 1A, SEM was utilized to show the surface topography of the triphasic composites and controls.


https://doi.org/10.1021/acsami.4c14712
ACS Appl. Mater. Interfaces 2025, 17, 3852−3865

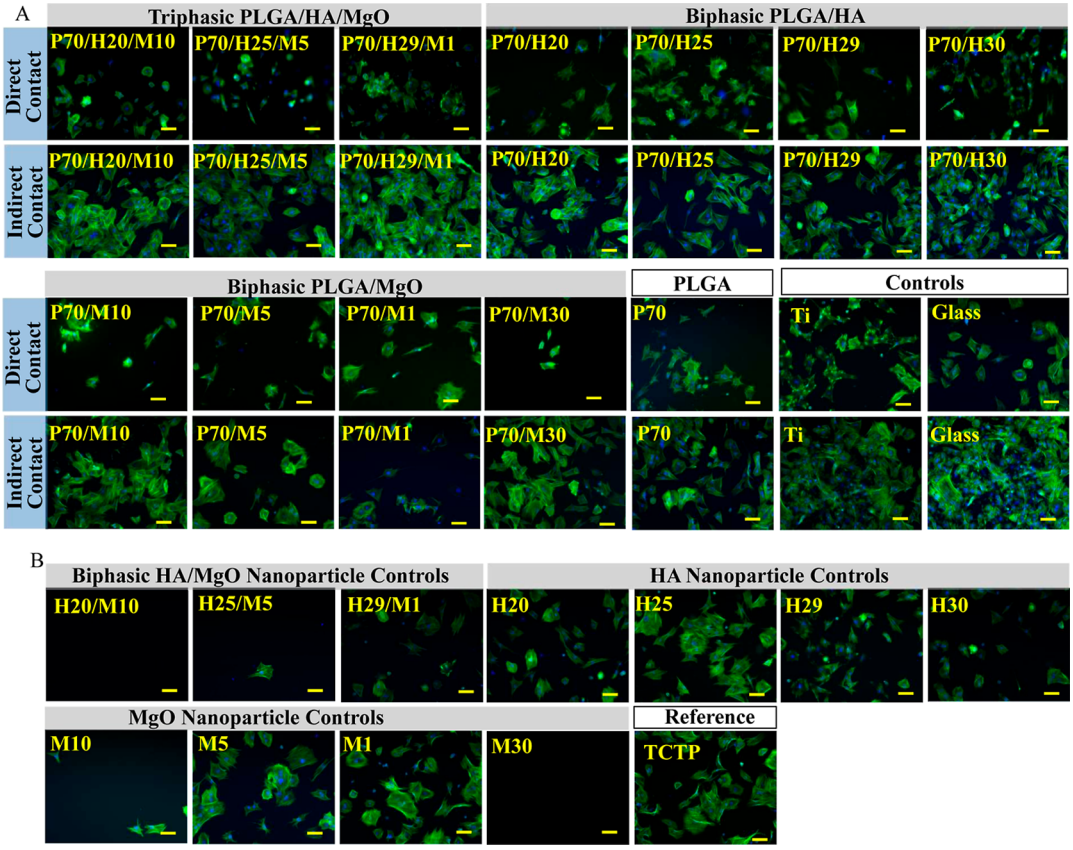


**Figure 2.** Representative fluorescence images of BMSCs after 24 h of direct culture. (A) BMSCs adhered directly to the scaffolds of interest and controls and to TCTP surrounding the scaffolds and controls. (B) BMSCs cultured with nanoparticle controls and BMSCs in the reference group. Scale bar is 100 $\mu$m.

All three triphasic nanocomposites of P70/H20/M10, P70/H25/M5, and P70/29/M1 exhibited homogeneous distribution of nanoparticles, though P70/H20/M10 and P70/H25/M5 had larger agglomerates than P70/H29/M1. Biphasic PLGA/HA and PLGA/MgO controls also exhibited an even distribution of visible nanoparticles. As shown in Figure 1B, EDS was utilized to confirm the elemental composition of each nanocomposite. As expected, all the triphasic and biphasic nanocomposites and PLGA control showed atomic percentages of different elements that were consistent with their designed composition.

**3.2. Cell Morphology and Adhesion Density after Culture with Nanocomposites and Controls.** Figure 2 shows representative fluorescence images of cells that were adhered to the samples (direct contact) and to the well-plate surrounding the respective samples (indirect contact) as well as cells in the groups of nanoparticle controls and cell-only reference after 24 h of direct culture. As shown in Figure 2A, BMSCs adhered on each triphasic PLGA/HA/MgO nanocomposite, biphasic nanocomposite, control, and reference and all showed normal morphology. Cells that adhered to the plate surrounding the samples also exhibited normal morphology. However, the group with the highest MgO content (P70/M30) showed visibly fewer cells with a relatively smaller cell spreading area than the other groups. Figure 2B shows that both nanoparticle controls of HA/MgO and MgO-only groups exhibited MgO dose-dependent BMSC adhesion densities. Specifically, nanoparticle groups with a higher MgO concentration such as H20/M10, M30, and M10 showed fewer adhered cells than their counterparts with lower MgO concentrations such as H29/M1, M5, and M1.

Figure 3 shows representative fluorescence images of cells that were adhered to the samples (direct contact) and to the well-plate surrounding the respective samples (indirect contact) as well as cells in the groups of nanoparticle controls and cell-only reference after 48 h of direct culture. As shown in Figure 3A, BMSCs in direct and indirect contact with the respective samples all exhibited normal morphology after 48 h of direct culture. The cell number in each image taken after 48 h of direct culture was greater than its corresponding number taken after 24 h, because of cell proliferation over time. In the groups of triphasic nanocomposites, cells under direct and indirect contact conditions were abundant with approximate confluency ranging from 80 to 90%. In Figure 3B, visibly fewer cells were found in the nanoparticle groups of H25/M5 and H29/M1 compared to those in the other groups. Images are not shown for the nanoparticle groups where no cells were found, such as H20/M10, M10, and M30.

Figure 4A and Table S1 show quantitative BMSC adhesion density under direct and indirect contact conditions after 24 h of direct culture. Under direct contact conditions, all the groups of polymer/ceramic nanocomposites and polymer control exhibited significantly lower cell adhesion density compared to Ti and Glass references. Among the triphasic nanocomposites, the P70/H29/M1 group showed the highest average cell adhesion density. The P70/H29/M1 group also had a statistically higher cell adhesion density than its biphasic nanocomposite controls of P70/H29 and P70/M1. Moreover,


https://doi.org/10.1021/acsami.4c14712
ACS Appl. Mater. Interfaces 2025, 17, 3852−3865

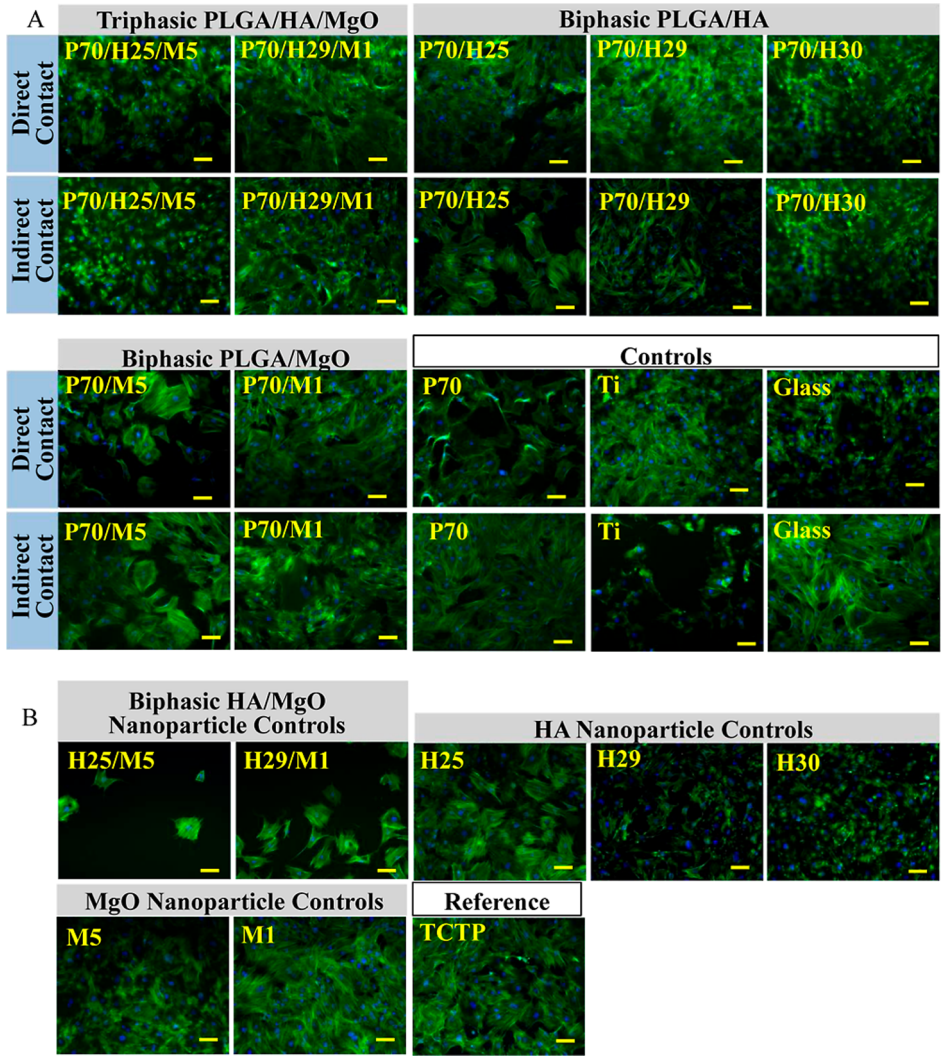


**Figure 3.** Representative fluorescence images of BMSCs after 48 h of direct culture. (A) BMSCs adhered directly to the scaffolds of interest and controls and to TCTP surrounding the scaffolds and controls. (B) BMSCs cultured with nanoparticle controls and BMSCs in the reference group. Scale bar is 100 $\mu$m.

the groups of biphasic nanocomposites exhibited nanoparticle dose-dependent BMSC adhesion densities on the samples. For instance, the groups of P70/H30 and P70/H29 had lower average cell adhesion densities than groups of P70/H25 and P70/H20; and the groups of P70/M30 and P70/M10 exhibited lower average cell adhesion densities than P70/M5 and P70/M1. Under indirect contact conditions, the cell adhesion density on the triphasic samples increased when decreasing the MgO concentration in the nanocomposite, and P70/H29/M1 group showed the highest average cell adhesion density among the triphasic nanocomposites. Both triphasic groups of P70/H25/M5 and P70/H20/M10 showed higher average cell adhesion densities than its biphasic controls, while the triphasic group of P70/H29/M1 had lower average cell adhesion density than its biphasic control of P70/H29. In average, all the triphasic groups showed higher cell adhesion densities than their corresponding nanoparticle controls. The nanoparticle groups of M30 and M10 showed near to 0 viable cells.

The quantified cell adhesion density after 48 h of culture is shown in Figure 4B. Under direct contact conditions, on average, cell adhesion densities on triphasic groups were higher than that of their corresponding biphasic groups. The P70/H29/M1 showed a higher average cell adhesion density than P70/H25/M5, but no statistical difference was detected. Under indirect contact conditions, the triphasic group of P70/H29/M1 showed higher average cell adhesion density than its biphasic controls, while the triphasic group of P70/H25/M5 had lower cell adhesion density than its biphasic control of P70/H25. P70/H29/M1 showed a higher average cell adhesion density than P70/H25/M5, but no statistical difference was detected. All groups of nanoparticles, except for M1, showed a significant decrease in cell adhesion density when compared to Glass and TCTP references.

**3.3. Postculture Medium Analysis for pH and $Mg^{2+}$ and $Ca^{2+}$ Concentrations.** As shown in Figure 5A and Table S2, the pH of media differed between the samples after 24 and 48 h of culture. After 24 h of culture, the average pH values of media in the triphasic nanocomposite groups were higher in a range of 8.25−8.37, and the values increased with increasing MgO content in the nanocomposites. As expected, the M30 group had the highest pH value, which was statistically greater than all other samples. After 48 h of culture, the pH value of all the groups was lower in a range of 7.8−7.95, possibly because


https://doi.org/10.1021/acsami.4c14712
ACS Appl. Mater. Interfaces 2025, 17, 3852−3865

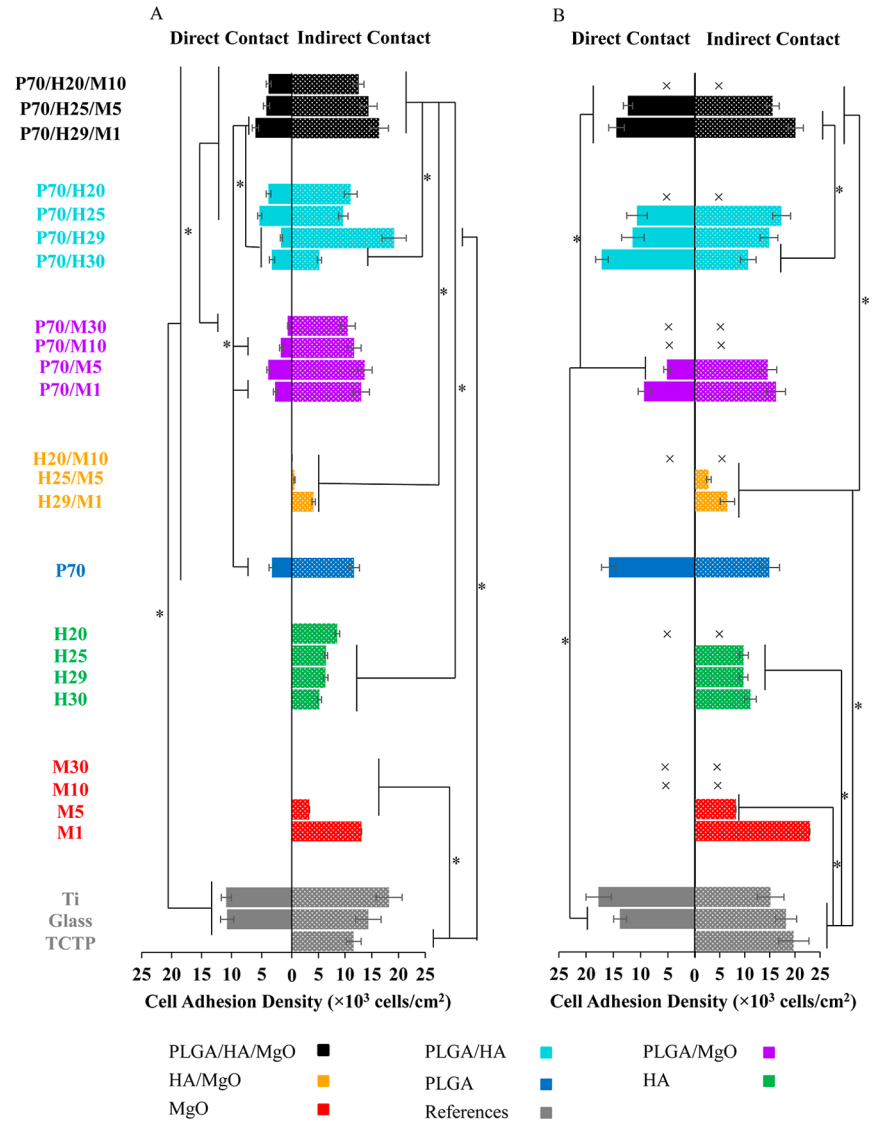


**Figure 4.** Quantitative adhesion density of BMSCs after 24 and 48 h of direct culture. (A) BMSC adhesion density under direct (left bar graph) and indirect (right bar graph) contact conditions after 24 h of direct culture. (B) BMSC adhesion density under direct (left bar graph) and indirect (right bar graph) contact conditions after 48 h of direct culture. Values are shown as mean ± standard deviation ($n$ = 3); *$p$ < 0.05.

of the reduction in $OH^-$ ion release and the presence of the bicarbonate buffer in the media.

As shown in Figure 5B and Table S2, the release of $Mg^{2+}$ ions corresponded with the amount of MgO in samples cultured for 24 h. As expected, the groups with higher MgO content showed a higher $Mg^{2+}$ concentration in the media, and all the groups without MgO exhibited similar $Mg^{2+}$ concentration in the media. After 48 h of culture, the $Mg^{2+}$ ion concentrations in the triphasic nanocomposite groups and the biphasic nanocomposite groups increased, but the trend among different samples was similar to that in 24 h of culture.

$Ca^{2+}$ concentrations in the media after 24 h of culture are shown in Figure 5C and Table S2. All the polymer/ceramic nanocomposite groups showed a similar $Ca^{2+}$ concentration in the media. All the nanoparticle groups, except for M1, had lower average $Ca^{2+}$ concentration than their polymer/ceramic nanocomposite counterparts and references of TCTP and DMEM. After 48 h of culture, the general trend of $Ca^{2+}$ concentration among different samples was similar to that in 24 h of culture. After 48 h of culture, the $Ca^{2+}$ ion concentrations of triphasic nanocomposites of P70/H25/M5 and P70/H29/M1 decreased slightly when compared with that after 24 h.

**3.4. Degradation Behavior of PLGA/HA/MgO over 28 Days of Immersion.** As shown in Figure 6 and Table S3, all PLGA-based nanocomposites showed significant mass loss over 28 days. During degradation, the physical appearance of each nanocomposite and polymer control changed over time, as shown in Figure S1. Specifically, all the samples showed increased opacity over the 28-day submersion. PLGA degrades through hydrolysis of its ester linkages, leading to the observed increase in opacity.[39,40] Samples with higher MgO content, particularly P70/H20/M10 and P70/M30, became more fragile after 14 and 28 days of degradation. Two of the three samples of P70/H20/M10 and one of the P70/M30 samples broke into several pieces that could no longer be handled after 28 days and are therefore not included in Figure S1. MgO containing samples of PLGA/HA/MgO and PLGA/MgO nanocomposites exhibited a MgO concentration-dependent degradation rate. Specifically, for triphasic nanocomposites, the


https://doi.org/10.1021/acsami.4c14712
ACS Appl. Mater. Interfaces 2025, 17, 3852−3865

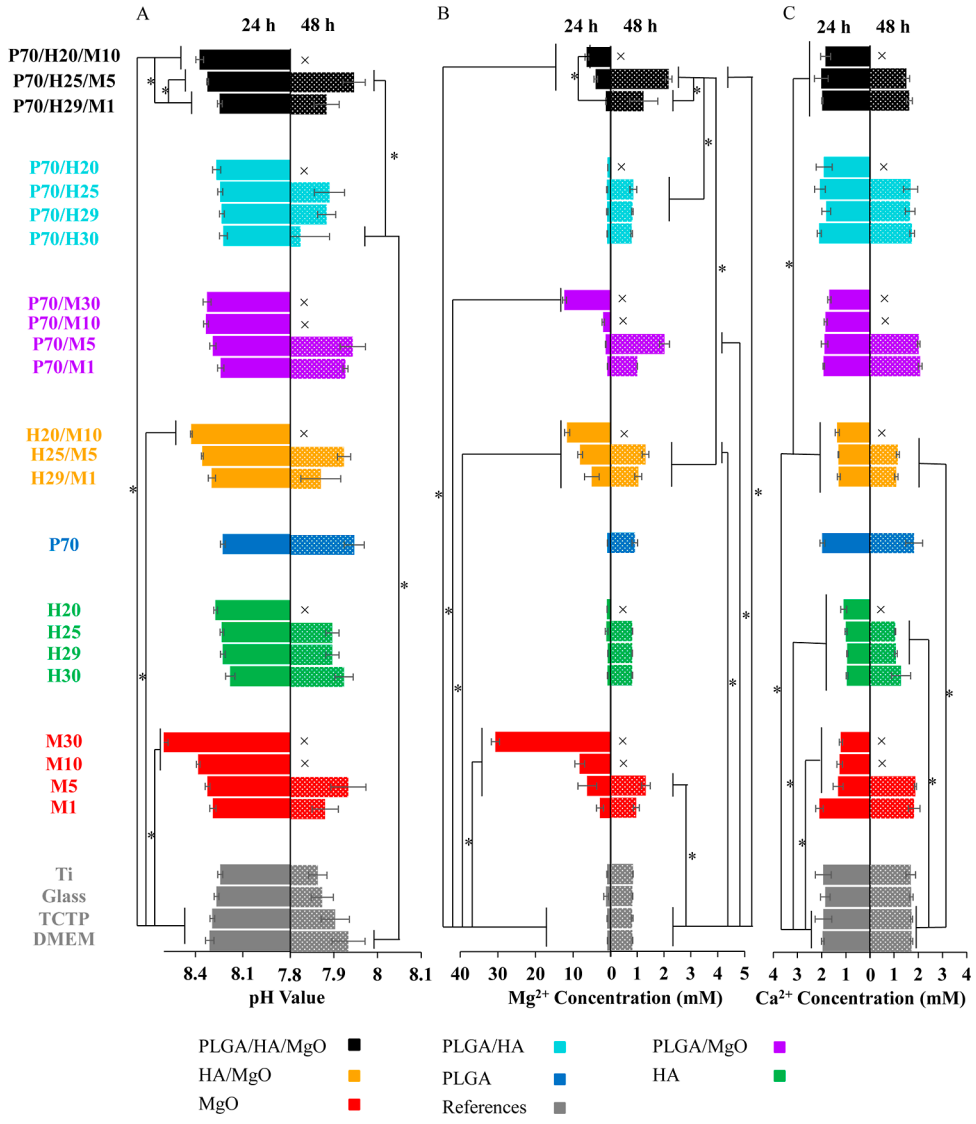


**Figure 5.** Analyses of postculture media after BMSC culture with triphasic and biphasic nanocomposites and controls. (A) pH values of media after 24 h (left bar graph) and 48 h (right bar graph) of culture. (B) $Mg^{2+}$ ion concentration in the media after 24 h (left bar graph) and 48 h (right bar graph) of culture. (C) $Ca^{2+}$ ion concentration in the media after 24 h (left bar graph) and 48 h (right bar graph) of culture. Values are shown as mean ± standard deviation ($n$ = 3); *$p$ < 0.05.

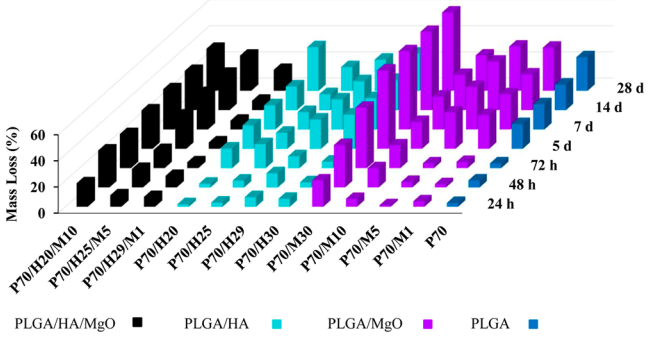


**Figure 6.** Degradation behavior of triphasic and biphasic nanocomposites and PLGA control. The 3D graph showing the percent mass loss of the nanocomposites and PLGA control to their initial mass, after each prescribed time point over 28 days of degradation in DMEM without cells (acellular conditions).

samples with higher MgO concentration exhibited greater mass loss at all the time points. Among PLGA/MgO nanocomposites, P70/M30 showed the greatest mass loss over 28 days of immersion. Interestingly, all the MgO-containing samples underwent a rapid mass loss after 24 h of immersion, followed by a subsequent slowing of degradation. Biphasic nanocomposite of P70/M30 degraded faster than that of P70/H30.

Figure 7 shows media analyses after each prescribed time point up to 28 days of culture with each composite and control under acellular conditions. In general, the pH value of all the samples gradually decreased over the 28 days, and the values were in the range of 7.9−8.7, as shown in Figure 7A and Table S4. Samples with bare MgO resulted in a significant increase in pH when compared with the TCTP control over 14 days of immersion. The increase in pH from these groups of nanoparticles diminished at later time points, and no statistical difference was detected between these samples and TCTP control after 28 days. As shown in Figure 7B and Table S5, as expected, MgO-containing samples showed a significant increase in $Mg^{2+}$ concentration when compared to other


https://doi.org/10.1021/acsami.4c14712
ACS Appl. Mater. Interfaces 2025, 17, 3852−3865

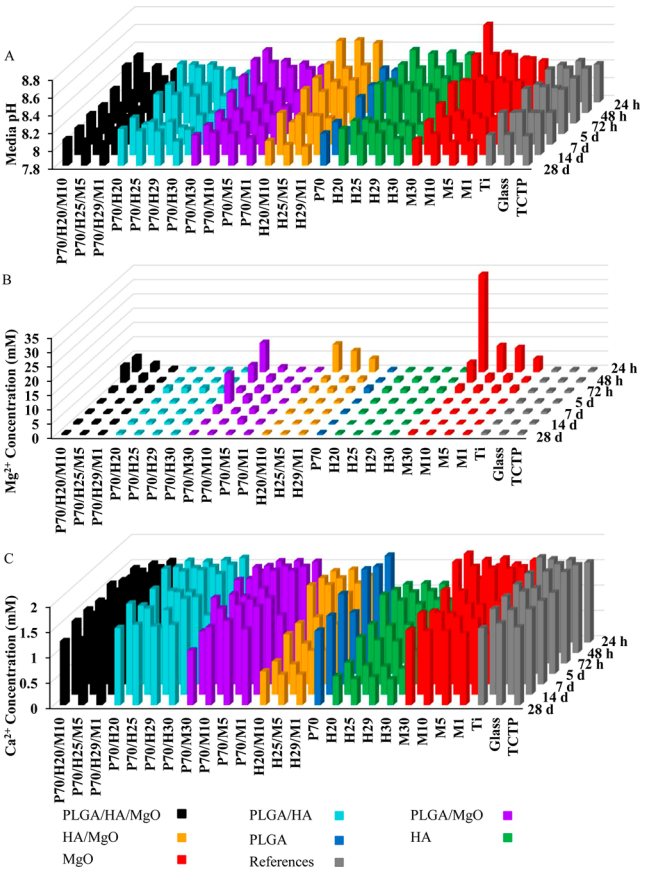


**Figure 7.** Media analyses after each prescribed time point up to 28 days of culture with each composite and control in acellular conditions. (A) pH values of media. (B) $Mg^{2+}$ ion concentration in the media. (C) $Ca^{2+}$ ion concentration in the media. Values are shown as mean ± standard deviation ($n$ = 3); *$p$ < 0.05.

sample groups and the TCTP reference. Overall, the highest $Mg^{2+}$ concentrations of MgO-containing sample groups were measured after 24 h of immersion in DMEM, indicating the burst release of $Mg^{2+}$ ions. Interestingly, P70/M30 showed cycles of rapid increase and decrease of $Mg^{2+}$ concentrations over 28 days, indicating multiple phases of degradation and $Mg^{2+}$ release. Figure 7C and Table S6 show that all of the HA containing groups, especially HA and HA/MgO nanoparticle groups, exhibited a decrease of $Ca^{2+}$ concentration in the media over 28 days, indicating that these materials may increase the calcium depositions.

**3.5. Improved Nanoparticle Dispersion Is Important for Microstructure and Properties of Nanocomposites.** As demonstrated in the materials science tetrahedron for a given application, the performance, property, micro-to-nano structure, and processing of a material are interrelated. The incorporation of bioactive nanoparticles such as HA and MgO into the PLGA matrix alters the composition, bioactivity, surface morphology, hydrophilicity, microstructure, and degradation behavior of triphasic nanocomposites, thus providing tunability for their performance in bone tissue regeneration. Distribution of the nanoparticles may significantly affect the above-mentioned properties. For example, Wetteland and Liu reported that PLGA (LA/GA = 50:50) with 30 wt % agglomerated MgO nanoparticles showed significantly higher cell adhesion density than PLGA with 30 wt % well-dispersed MgO nanoparticles.[18] This is because well-dispersed MgO nanoparticles increased direct contact of MgO with BMSCs and the high-level direct exposure of MgO on the top surface is detrimental to cells.[18] In order to optimize the concentration and ratio of nanoparticles in nanocomposites, it is crucial to achieve a homogeneous dispersion of nanoparticles within the polymeric matrix and thus minimize the variability resulting from agglomeration. However, nanoparticles have relatively high specific surface areas, and their addition to a polymer solution would dramatically increase the viscosity of the slurry, which might be detrimental to its uniform distribution in the composites. Nanoparticles such as MgO can further increase the viscosity of the slurry because of the interactions between nanoparticles and polyesters.[37] The mechanical approach of integrating high-power sonication and DAC speed mixing enhanced the dispersion of nanoparticles in the composites. Our previous study demonstrated that the integration of these two mixing processes significantly enhanced uniform dispersion of respective HA and MgO nanoparticles in PLGA matrix when compared with the traditional high-power sonication only approach.[18] The mechanical mixing approach avoided the toxicity concerns associated with chemical-based surface modification approaches for improving the dispersion of nanoparticles. The synergistic regulation of HA and MgO on the degradation behavior and in vivo osteogenesis of PLGA/HA/MgO composites are beneficial for bone tissue regeneration.[41] In addition to composition, the dispersion of nanoparticles played important roles in the microstructure and properties of triphasic nanocomposites, such as biodegradation behavior and cell−material interactions.

**3.6. Discussion on the Factors Affecting the Degradation of Nanocomposites—PLGA Composition, *n*HA, *n*MgO, and Environment.** The degradation of triphasic PLGA/HA/MgO nanocomposites involves degradation of PLGA as well as dissociation of MgO and HA nanoparticles, as shown in Figure 8A. Upon exposure to cell culture media, MgO nanoparticles started to dissociate and release degradation products, such as $OH^-$ and $Mg^{2+}$ ions, when exposed to water. Because of water diffusion, the PLGA matrix started to degrade through hydrolysis of its ester linkages and exhibit the mode of bulk erosion. The dissociation of MgO and release of MgO and HA nanoparticles occurred continuously during the polymer degradation. HA nanoparticles utilized in this study had relatively high crystallinity due to the hydrothermal treatment. It may take months or years for the released HA nanoparticles to degrade completely.[42]

The PLGA matrix and the incorporated HA and MgO nanoparticles determined the degradation rate of triphasic nanocomposites interdependently, as shown in Figure 8B. For the polymeric matrix of PLGA, the degradation rate is tunable by varying the ratio of LA to GA.[43] Specifically, Miller et al. reported that the degradation rate of PLGA increased and then dropped, when increasing the ratio of LA/GA.[43] At a LA/GA ratio of 50:50, PLGA showed the greatest degradation rate.[43] PLA is a type of hydrophobic material that has low water diffusion, exhibiting relatively slow hydrolytic decomposition. PGA has a high crystallinity of 45−55%, also resulting in a comparatively low degradation rate. The blending of PLA and PGA balances the hydrophobicity and crystallinity of PLGA, leading to the highest degradation rate at an LA/GA ratio of 50:50. PLGA utilized in this article had a LA/GA ratio of


https://doi.org/10.1021/acsami.4c14712
ACS Appl. Mater. Interfaces 2025, 17, 3852−3865

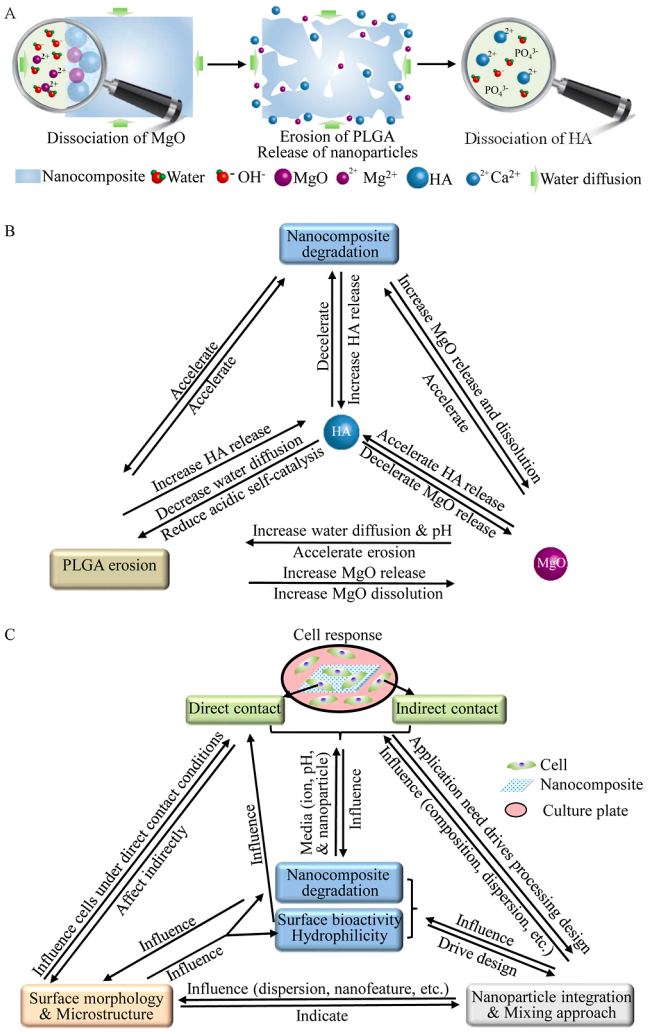


**Figure 8.** Effects of nanoparticle incorporation on degradation behavior of triphasic nanocomposites and cell responses. (A) Degradation process of triphasic nanocomposites. (B) Schematic diagram showing the inter-relations among HA, MgO, PLGA erosion, and nanocomposite degradation. (C) Schematic diagram showing the inter-relations among processing, property, micro-to-nano structure, and performance (i.e., cell response) of triphasic nanocomposites.

90:10, and the hydrophobicity decreased the water diffusion, as well as the degradation rate.

The incorporation of nanoparticles could accelerate or decelerate the process of polymer erosion. Previous research has indicated that the addition of HA decreased the degradation rate of several polymers such as PLGA (LA/GA = 50:50),[44] PLLA,[45] and PLA.[46] On the one hand, HA is a material with a relatively low dissociation rate, and the addition of HA helps reduce the water diffusion in polymer nanocomposites. On the other hand, degradation of PLGA results in the generation of acidic products, and HA embedded in the polymeric matrix may reduce the possibility of acidic self-catalysis effect, thus decelerating the degradation of composites.[45] MgO incorporated in the PLGA matrix, however, has been demonstrated to accelerate the degradation of the composite.[41] The hygroscopic nature of MgO contributed to water diffusion in the nanocomposite, accelerating the hydrolytic decomposition of ester linkages in PLGA. Moreover, the dissociation of MgO resulted in the release of $OH^-$ ions, which neutralized the acidic degradation products of PLGA and then increased the pH of the medium to an alkaline level. The elevated pH of the media can accelerate the hydrolysis process of ester bond.[47] The bicarbonate buffer in the media attenuated the influence of MgO nanoparticles on pH change (Figure 7A and Table S4), which is consistent to our previous results.[18,36] Our previous study on bare MgO and $Mg(OH)_2$ found that these nanoparticles dissociated when exposed to DMEM. The dissociation of MgO and $Mg(OH)_2$ is pH-dependent.[48] Fruhwirth et al. showed that MgO dissociated at a pH of 7−8.5, with an overall reaction of $MgO + H_2O \rightarrow Mg^{2+} + 2\ (OH)^-$.[49] The buffer present in DMEM could modulate the pH to be in this range, thereby facilitating the dissociation of MgO. MgO is also known for its conversion to $Mg(OH)_2$ in water. However, the release of $Mg^{2+}$ from the nanocomposites was observed, similar to the behavior of bare MgO nanoparticles in DMEM, thus supporting the idea that MgO dissociated to ions eventually. MgO could have been either dissociated directly or dissociated after conversion to $Mg(OH)_2$. In our previous studies on bare MgO nanoparticles, $Mg(OH)_2$ was found in the remaining particles after bare MgO was immersed in DMEM,[48] and there are two possible processes for the formation of $Mg(OH)_2$. One possibility is precipitation of $Mg(OH)_2$ from $Mg^{2+}$ and $OH^-$ ions after MgO dissociated; and another possibility is conversion of MgO to $Mg(OH)_2$ due to hydration of their shared crystal face. However, both MgO and $Mg(OH)_2$ particles have been shown to dissociate in DMEM. For the nanocomposites, the pH and buffering effects of DMEM are more likely to have a greater effect on the overall degradation behaviors of nanocomposites than the possible intermediate conversion of MgO to $Mg(OH)_2$, since both MgO and $Mg(OH)_2$ eventually dissociated to ions in DMEM. The dissociation of MgO also explained why the MgO-containing samples underwent a rapid mass loss after 24 h of immersion, followed by a subsequent reduction of degradation rate during 28 days of immersion (Figure 6 and Table S3). Since HA and MgO showed opposing effects on the PLGA degradation, the degradation rate of the triphasic PLGA/HA/MgO nanocomposites is tunable by controlling the concentration and ratio of HA and MgO, as well as the LA/GA ratio of the PLGA matrix. In this study, well-dispersed MgO nanoparticles might have played a dominant role in accelerating the degradation process, since all the triphasic samples degraded faster than PLGA control (Figures S1 and 6).

In addition to intrinsic factors such as material composition, environmental factors can also influence the degradation behavior of the polymer/ceramic nanocomposites. For example, the presence of cells in the culture media may accelerate the degradation of some materials when compared with their counterparts cultured in the same media without cells. These materials can be degraded by enzymes, which are secreted by cells, similarly to how microorganisms degrade the biodegradable materials. Cells may also accelerate the metabolic processes of the degradation products, such as nanoparticles, short-chained polymers, and oligomers. For example, BMSCs cultured with the magnetic hyaluronic acid hydrogels can uptake the released magnetic nanoparticles during the degradation of the hydrogels.[50] Moreover, mineral deposition may form on the material surface during the degradation process, which could influence the degradation rate of the implant. For example, mineral depositions such as $Mg_3(PO_4)_2{\cdot}8H_2O$, $MgCO_3{\cdot}3H_2O$, and $CaCO_3$ were found on the Mg alloys of ZC21 and ZSr41 after the in vivo study, and


https://doi.org/10.1021/acsami.4c14712
ACS Appl. Mater. Interfaces 2025, 17, 3852−3865

these depositions could reduce the weight loss of the material.[10] In this article, the mineral deposition may decrease the degradation rate in HA-containing samples since all these sample groups showed decreased $Ca^{2+}$ ion concentration in the media after cell culture and degradation study, suggesting the formation of calcium-containing mineral deposition (Figures 5C and 7C).

**3.7. Discussion on the Cell Responses to Nanocomposites with *n*HA and *n*MgO.** Figure 8C illustrates the interactive relationships among the processing, nano-to-micro structure, property, and performance of cell response to triphasic nanocomposites. During the bone healing process, the implanted materials influence cells under both direct and indirect contact conditions. The direct culture method utilized in this article evaluated the responses of newly seeded cells that adhered to samples (direct contact) and to the well-plate surrounding the materials (indirect contact).[38]

Cells under direct contact conditions are influenced by multiple factors including material processing such as addition of nanoparticles and mixing techniques for integration and distribution, material structure such as surface morphology and microstructure, and material property such as surface bioactivity, surface hydrophilicity, and degradation rate.[51] Cells under indirect contact conditions, however, are mainly affected by media environments regulated by the degradation of materials. In recent decades, extensive studies have been conducted to investigate the effects of these factors on cell−material interactions. For example, Xu et al. reported that fibroblasts (NIH 3T3) seeded on the 4-arm poly(ethylene glycol)-*block*-poly(L-glutamic acid) hydrogels modified with arginylglycylaspartic acid (RGD) showed statistically greater adhesion density than cells on the hydrogels without RGD modification, indicating the effects of surface bioactivity on cell adhesion.[52] In another example, Khorasani et al. investigated the effects of hydrophilicity of polymer films on the cell responses. The results showed that B65 cells (from neural tissue) seeded on the $O_2$ plasma-treated PLLA and PLGA (PLA/PGA = 50:50) films (water contact angle: 10° for PLLA and 36.6° for PLGA) exhibited enhanced adhesion and proliferation than cells on their corresponding nontreated PLLA and PLGA films (water contact angle: 85° for PLLA and 74.5° for PLGA).[53] Moreover, Yang et al. reported that osteoblasts adhered on the spherical nanocrystalline diamond exhibited statistically greater spreading area than cells adhered on the chunky submicrometer-crystalline diamond and polyhedral/cubic micrometer-crystalline diamond, which suggested that cell responses were influenced by the surface microstructure and morphology.[54]

In this study, the above-mentioned factors in processing, surface, microstructure, and property could influence the cell responses interdependently since these factors are inter-related, as demonstrated in Figure 8C. For example, the mixing technique enhanced dispersion of HA and MgO nanoparticles; and the dispersion of nanoparticles in the PLGA matrix altered the surface morphology and microstructure of the nanocomposites. The addition of HA and MgO as bioactive components also modified the bioactivity of nanocomposites. The hydrophilic nature of HA and MgO nanoparticles enhanced surface hydrophilicity of nanocomposites. Moreover, the nanoparticle dispersion techniques, concentration and ratio of the nanoparticles, and PLGA type used in the processing determined the degradation rate of the nanocomposites, which has significant effects on cell−material interactions. The degradation behavior of the nanocomposites dominated the changes in cell culture media such as pH value, ion concentrations, and release of nanoparticles, which affects the cell responses under both direct and indirect contact conditions. For example, the dissociation of MgO nanoparticles elevated the pH of the media, while the acidic degradation products of PLGA decreased the pH value, and the changes in pH caused by nanocomposites with varying degradation rates affected the cell responses. Moreover, earlier research has shown that media containing 5−10 mM $Mg^{2+}$ ions ($MgSO_4$) enhanced BMSC proliferation when compared with the original cell culture media with 0.8 mM $Mg^{2+}$ ions.[55] The $Mg^{2+}$ ions released from the PLGA/HA/MgO nanocomposite (Figures 5B and 7B) were in a safe range. It has been reported that the culture media supplemented with up to 27.6 mM $Mg^{2+}$ ions did not induce any detectable adverse effects on BMSC responses.[35] In addition, nanoparticles had dose-dependent toxicity in cell cultures, as shown by the findings of the nanoparticle control groups (Figure 4). The degradation rate of the nanocomposite determined the release rate of nanoparticles into the media, thus influencing the cell responses. Moreover, the released nanoparticles had a higher contact area with media and cells when compared with their counterparts embedded in the polymeric matrix. The accelerated dissociation of these released nanoparticles also increased the pH and ion concentration in the media, which contributed to the observed cell−material interactions. In general, to control cell−material interactions, it is crucial to optimize the processing parameters to achieve the desired micro-to-nano structures of material and properties, especially considering the relationships of these factors, as illustrated in the materials science tetrahedron concept in Figure 8C.

To achieve the best performance in different bone tissue regeneration applications, multiple aspects, such as cell−material interactions, biodegradation rate, and bone healing time, should be considered comprehensively. For example, in the scenario where the bone healing process is relatively rapid (e.g., pediatric patients), triphasic nanocomposites with a higher MgO content such as P70/H20/M10 and P70/H25/M5 may be selected. Nanocomposites with a lower degradation rate, such as P70/H29/M1 may be utilized when the bone regeneration process is slower (e.g., elder patients). The appropriate concentration and ratio of HA and MgO nanoparticles in the nanocomposites may vary when a different polymeric matrix is utilized. For example, Hickey et al. investigated PLLA with 10% HA and 10% MgO and discovered an increase in the density of primary human osteoblasts compared to PLLA with 20% HA.[27] However, no statistical difference in cell adhesion density was detected between the groups of PLGA/HA/MgO with 10% MgO and 20% HA and PLGA/HA composites with 20% HA, after 24 and 48 h of culture in our study (Figure 5). This may be related to variations in degradation rates of two different polymers. PLGA tends to degrade more rapidly than PLLA, resulting in a greater rate of MgO release, which resulted in different cell responses. Moreover, nanocomposites with different porous structures or porosities may have different degradation rates due to variations in water diffusion capability. In this case, the concentration and ratio of nanoparticles in the nanocomposites should be modified to obtain the desired degradation rate.

**3.8. Future Directions.** This article provides critical information to optimize material composition and nanoparticle


https://doi.org/10.1021/acsami.4c14712
ACS Appl. Mater. Interfaces 2025, 17, 3852−3865

dispersion of triphasic nanocomposites for bone regeneration from the perspective of degradation and cell responses of nanocomposites. In the next step, osteogenic differentiation of BMSCs cultured on the PLGA/HA/MgO nanocomposites should be further evaluated in vitro using long-term culture and biochemical assays such as ALP activity, collagen assay, and calcium assay. The expression of osteogenic genes, such as RUNX2, osterix (Osx), and osteocalcin (OCN), may be studied using real-time PCR to further access the osteogenic capability of different nanocomposites. Moreover, the potential of these nanocomposites for bone regeneration should be assessed in vivo using relevant animal models such as the rodent calvarial defect model. New bone formation at the defect sites can be evaluated through microcomputed tomography, hematoxylin and eosin (H&E) staining, and Masson's trichrome staining. Immunohistochemistry (IHC) staining for OCN could be used to assess osteoblastic differentiation and mineralization in the future.

## 4. CONCLUSIONS

In this article, we successfully prepared triphasic PLGA/HA/MgO nanocomposites with improved nanoparticle dispersion by using a process that integrated the benefits of ultrasonic energy and DAC mixing. The as-prepared triphasic nanocomposites exhibited a homogeneous nanoparticle distribution and as-designed elemental composition. BMSC adhesion density under both direct and indirect contact conditions increased with decreasing MgO content in the triphasic nanocomposites. Moreover, MgO nanoparticles in the PLGA matrix accelerated the degradation of triphasic nanocomposites. Cell culture and degradation studies indicated that pH and $Mg^{2+}$ ion concentrations in the media increased when increasing the MgO content of the triphasic nanocomposites. This article evaluated the synergistic effects of HA and MgO on degradation behavior and cell−material interactions of triphasic nanocomposites and suggested that P70/H29/M1 may be used when the bone healing process is slow, while P70/H25/M5 or P70/H20/M10 may be considered when the bone healing is relatively rapid. The concentration and ratio of nanoparticles in different biodegradable polymers should be modified and fine-tuned based on the degradation behaviors of the polymeric matrix.

## ■ ASSOCIATED CONTENT

### Supporting Information

The Supporting Information is available free of charge at https://pubs.acs.org/doi/10.1021/acsami.4c14712.

Table showing cell density on the samples of interest and the tissue culture plate around the respective samples after 24 and 48 h of culture, table showing the pH value, $Mg^{2+}$ ion concentration, and $Ca^{2+}$ ion concentration from postculture media analyses after 24 and 48 h of BMSC culture, table showing percent mass loss of the triphasic PLGA/HA/MgO and controls to their initial mass, tables showing pH value, $Mg^{2+}$ ion concentration, and $Ca^{2+}$ ion concentration of media after each prescribed time point of culture with each composite and control in acellular conditions, and photographs showing nanocomposites and PLGA control over 28 days of immersion degradation in DMEM (PDF)

## ■ AUTHOR INFORMATION


### Corresponding Author

**Huinan Hannah Liu** − *Department of Bioengineering, Materials Science and Engineering Program, and Stem Cell Center, University of California, Riverside, Riverside, California 92521, United States;* orcid.org/0000-0001-9366-6204; Phone: 951-827-2944; Email: huinan.liu@ucr.edu; Fax: 951-827-6416

### Authors

**Cheyann Wetteland** − *Department of Bioengineering, University of California, Riverside, Riverside, California 92521, United States*

**Changlu Xu** − *Materials Science and Engineering Program, University of California, Riverside, Riverside, California 92521, United States;* orcid.org/0000-0001-5968-2462

**Sebo Michelle Wang** − *Department of Bioengineering, University of California, Riverside, Riverside, California 92521, United States*

**Chaoxing Zhang** − *Materials Science and Engineering Program, University of California, Riverside, Riverside, California 92521, United States;* orcid.org/0000-0003-4115-7111

**Elizabeth Juntilla Ang** − *Department of Bioengineering, University of California, Riverside, Riverside, California 92521, United States*

**Cole Gabriel Azevedo** − *Materials Science and Engineering Program, University of California, Riverside, Riverside, California 92521, United States*

Complete contact information is available at: https://pubs.acs.org/10.1021/acsami.4c14712


### Notes

The authors declare no competing financial interest.

## ■ ACKNOWLEDGMENTS

The authors thank the partial support from the U.S. National Science Foundation (NSF award CBET 1125801), the Hellman Faculty Fellowship (HL), University of California (UC) Regents Faculty Development Award (HL), and the U.S. Department of Education for Hispanic Service Institutions Undergraduate Research Program (Award P031C110131, for supporting E.J.A.). The authors appreciate the Central Facility for Advanced Microscopy and Microanalysis (CFAMM) for the use of SEM FEI XL30 at the University of California at Riverside. Any opinions, findings, and conclusions or recommendations expressed in this material are those of the author(s) and do not necessarily reflect the views of the funding agencies.

## ■ REFERENCES

(1) Iaquinta, M. R.; Mazzoni, E.; Manfrini, M.; D'Agostino, A.; Trevisiol, L.; Nocini, R.; Trombelli, L.; Barbanti-Brodano, G.; Martini, F.; Tognon, M. Innovative biomaterials for bone regrowth. *Int. J. Mol. Sci.* **2019**, *20* (3), 618.

(2) Schmidt, A. H. Autologous bone graft: Is it still the gold standard? *Injury* **2021**, *52*, S18−S22.

(3) Betz, R. R. Limitations of autograft and allograft: new synthetic solutions. *Orthopedics* **2002**, *25* (5), S561−S570.

(4) Delloye, C.; Cornu, O.; Druez, V.; Barbier, O. Bone allografts: what they can offer and what they cannot. *J. Bone Jt. Surg., Br. Vol.* **2007**, *89-B* (5), 574−580.

(5) Li, Z.; Kang, M.; Xu, C.; Chiang, M.; Lee, C.-S.; Lee, M. Black Phosphorus-Based Dynamic Self-Healing Hydrogel to Integrate Demineralized Bone Matrix and Noggin-Targeting siRNA for Synergistic Osteogenesis. *ACS Appl. Mater. Interfaces* **2024**, *16* (18), 22874−22886.
(6) Chen, C.; Li, Z.; Xu, C.; Kang, M.; Lee, C. S.; Aghaloo, T.; Lee, M. Self-Assembled Nanocomposite Hydrogels as Carriers for Demineralized Bone Matrix Particles and Enhanced Bone Repair. *Adv. Healthcare Mater.* **2024**, *13* (10), 2303592.
(7) Liu, Y.; Xu, C.; Gu, Y.; Shen, X.; Zhang, Y.; Li, B.; Chen, L. Polydopamine-modified poly (l-lactic acid) nanofiber scaffolds immobilized with an osteogenic growth peptide for bone tissue regeneration. *RSC Adv.* **2019**, *9* (21), 11722−11736.
(8) Xu, C.; Bai, Y.; Yang, S.; Yang, H.; Stout, D. A.; Tran, P. A.; Yang, L. A versatile three-dimensional foam fabrication strategy for soft and hard tissue engineering. *Biomed. Mater.* **2018**, *13* (2), 025018.
(9) Xu, C.; Liu, H.; Yang, H.; Yang, L. A green biocompatible fabrication of highly porous functional ceramics with high strength and controllable pore structures. *J. Mater. Sci. Technol.* **2016**, *32* (8), 729−732.
(10) Zhang, C.; Lin, J.; Nguyen, N.-Y. T.; Guo, Y.; Xu, C.; Seo, C.; Villafana, E.; Jimenez, H.; Chai, Y.; Guan, R.; et al. Antimicrobial bioresorbable Mg−Zn−Ca alloy for bone repair in a comparison study with Mg−Zn−Sr alloy and pure Mg. *ACS Biomater. Sci. Eng.* **2019**, *6* (1), 517−538.
(11) Farazin, A.; Akbari Aghdam, H.; Motifard, M.; Aghadavoudi, F.; Kordjamshidi, A.; Saber-Samandari, S.; Esmaeili, S.; Khandan, A. A polycaprolactone bio-nanocomposite bone substitute fabricated for femoral fracture approaches: Molecular dynamic and micromechanical Investigation. *J. Nanoanal.* **2019**, *6* (3), 172−184.
(12) Liu, H.; Slamovich, E. B.; Webster, T. J. Increased osteoblast functions on nanophase titania dispersed in poly-lactic-co-glycolic acid composites. *Nanotechnology* **2005**, *16* (7), S601.
(13) Matassi, F.; Nistri, L.; Paez, D. C.; Innocenti, M. New biomaterials for bone regeneration. *Clin. Cases Miner. Bone Metab.* **2011**, *8* (1), 21−24.
(14) Jin, S.; Xia, X.; Huang, J.; Yuan, C.; Zuo, Y.; Li, Y.; Li, J. Recent advances in PLGA-based biomaterials for bone tissue regeneration. *Acta Biomater.* **2021**, *127*, 56−79.
(15) Wang, H. *Hydroxyapatite Degradation and Biocompatibility*; The Ohio State University, 2004.
(16) Murugan, R.; Ramakrishna, S. Development of nanocomposites for bone grafting. *Compos. Sci. Technol.* **2005**, *65* (15−16), 2385−2406.
(17) Liu, H.; Slamovich, E. B.; Webster, T. J. Increased osteoblast functions among nanophase titania/poly (lactide-co-glycolide) composites of the highest nanometer surface roughness. *J. Biomed. Mater. Res., Part A* **2006**, *78A* (4), 798−807.
(18) Wetteland, C. L.; Liu, H. Optical and biological properties of polymer-based nanocomposites with improved dispersion of ceramic nanoparticles. *J. Biomed. Mater. Res., Part A* **2018**, *106* (10), 2692−2707.
(19) Huang, Y.; He, J.; Gan, L.; Liu, X.; Wu, Y.; Wu, F.; Gu, Z. W. Osteoconductivity and osteoinductivity of porous hydroxyapatite coatings deposited by liquid precursor plasma spraying: in vivo biological response study. *Biomed. Mater.* **2014**, *9* (6), 065007.
(20) Jang, C. H.; Cho, Y. B.; Choi, C. H.; Jang, Y. S.; Jung, W. K.; Lee, J. K. Comparision of osteoconductivity of biologic and artificial synthetic hydroxyapatite in experimental mastoid obliteration. *Acta Otolaryngol.* **2014**, *134* (3), 255−259.
(21) Lin, L.; Chow, K. L.; Leng, Y. Study of hydroxyapatite osteoinductivity with an osteogenic differentiation of mesenchymal stem cells. *J. Biomed. Mater. Res. A* **2009**, *89A* (2), 326−335.
(22) Farzadi, A.; Solati-Hashjin, M.; Bakhshi, F.; Aminian, A. Synthesis and characterization of hydroxyapatite/$\beta$-tricalcium phosphate nanocomposites using microwave irradiation. *Ceram. Int.* **2011**, *37* (1), 65−71.
(23) Bellucci, D.; Sola, A.; Gazzarri, M.; Chiellini, F.; Cannillo, V. A new hydroxyapatite-based biocomposite for bone replacement. *Mater. Sci. Eng. C* **2013**, *33* (3), 1091−1101.
(24) Nabiyouni, M.; Ren, Y.; Bhaduri, S. B. Magnesium substitution in the structure of orthopedic nanoparticles: A comparison between amorphous magnesium phosphates, calcium magnesium phosphates, and hydroxyapatites. *Mater. Sci. Eng., C* **2015**, *52*, 11−17.
(25) He, L.; Zhang, X.; Liu, B.; Tian, Y.; Ma, W. Effect of magnesium ion on human osteoblast activity. *Braz. J. Med. Biol. Res.* **2016**, *49* (7), No. e5257.
(26) Khandaker, M.; Li, Y.; Morris, T. Micro and nano MgO particles for the improvement of fracture toughness of bone-cement interfaces. *J. Biomech.* **2013**, *46* (5), 1035−1039.
(27) Hickey, D. J.; Ercan, B.; Sun, L.; Webster, T. J. Adding MgO nanoparticles to hydroxyapatite-PLLA nanocomposites for improved bone tissue engineering applications. *Acta Biomater.* **2015**, *14*, 175−184.
(28) Roh, H. S.; Lee, C. M.; Hwang, Y. H.; Kook, M. S.; Yang, S. W.; Lee, D.; Kim, B. H. Addition of MgO nanoparticles and plasma surface treatment of three-dimensional printed polycaprolactone/hydroxyapatite scaffolds for improving bone regeneration. *Mater. Sci. Eng., C* **2017**, *74*, 525−535.
(29) Pourdanesh, F.; Jebali, A.; Hekmatimoghaddam, S.; Allaveisie, A. In vitro and in vivo evaluation of a new nanocomposite, containing high density polyethylene, tricalcium phosphate, hydroxyapatite, and magnesium oxide nanoparticles. *Mater. Sci. Eng., C* **2014**, *40*, 382−388.
(30) Wetteland, C. L.; Nguyen, N.-Y. T.; Liu, H. Concentration-dependent behaviors of bone marrow derived mesenchymal stem cells and infectious bacteria toward magnesium oxide nanoparticles. *Acta Biomater.* **2016**, *35*, 341−356.
(31) Choi, J.-S.; Seo, K.; Yoo, J.-W. Recent advances in PLGA particulate systems for drug delivery. *J. Pharm. Invest.* **2012**, *42* (3), 155−163.
(32) Liu, H.; Slamovich, E. B.; Webster, T. J. Less harmful acidic degradation of poly (lactic-co-glycolic acid) bone tissue engineering scaffolds through titania nanoparticle addition. *Int. J. Nanomed.* **2006**, *1* (4), 541.
(33) Schwendeman, S. P.; Shah, R. B.; Bailey, B. A.; Schwendeman, A. S. Injectable controlled release depots for large molecules. *J. Controlled Release* **2014**, *190*, 240−253.
(34) Chaurasia, M.; Singh, R.; Sur, S.; Flora, S. A review of FDA approved drugs and their formulations for the treatment of breast cancer. *Front. Pharm.* **2023**, *14*, 1184472.
(35) Cipriano, A. F.; Sallee, A.; Guan, R. G.; Zhao, Z. Y.; Tayoba, M.; Sanchez, J.; Liu, H. Investigation of magnesium-zinc-calcium alloys and bone marrow derived mesenchymal stem cell response in direct culture. *Acta Biomater.* **2015**, *12*, 298−321.
(36) Johnson, I.; Akari, K.; Liu, H. Nanostructured hydroxyapatite/poly (lactic-co-glycolic acid) composite coating for controlling magnesium degradation in simulated body fluid. *Nanotechnology* **2013**, *24* (37), 375103.
(37) Alvey, F. B. Study of the Reaction of Polyester Resins with Magnesium Oxide. *J. Polym. Sci., Part A: Gen. Pap.* **1971**, *9* (8), 2233−2245.
(38) Xu, C.; Chen, Y.; Lin, J.; Liu, H. H. Direct and indirect culture methods for studying biodegradable implant materials In Vitro. *J. Visualized Exp.* **2022**, No. 182, No. e63065.
(39) Gentile, P.; Chiono, V.; Carmagnola, I.; Hatton, P. V. An overview of poly(lactic-co-glycolic) acid (PLGA)-based biomaterials for bone tissue engineering. *Int. J. Mol. Sci.* **2014**, *15* (3), 3640−3659.
(40) Makadia, H. K.; Siegel, S. J. Poly Lactic-co-Glycolic Acid (PLGA) as Biodegradable Controlled Drug Delivery Carrier. *Polymers* **2011**, *3* (3), 1377−1397.
(41) Xia, X.; Huang, J.; Wei, J.; Jin, S.; Zou, Q.; Zuo, Y.; Li, J.; Li, Y. Magnesium oxide regulates the degradation behaviors and improves the osteogenesis of poly (lactide-co-glycolide) composite scaffolds. *Compos. Sci. Technol.* **2022**, *222*, 109368.

(42) Jin, H.-H.; Kim, D.-H.; Kim, T.-W.; Park, H.-C.; Yoon, S.-Y. Degradation Behavior of Hydroxyapatite with Different Crystallinity in Simulated Body Fluid Solution. *Korean J. Mater. Res.* **2011**, *21* (6), 347−351.
(43) Miller, R. A.; Brady, J. M.; Cutright, D. E. Degradation rates of oral resorbable implants (polylactates and polyglycolates): rate modification with changes in PLA/PGA copolymer ratios. *J. Biomed. Mater. Res.* **1977**, *11* (5), 711−719.
(44) Ege, D.; Cameron, R.; Best, S. The degradation behavior of nanoscale HA/PLGA and α-TCP/PLGA composites. *Bioinspired, Biomimetic Nanobiomater.* **2014**, *3* (2), 85−93.
(45) Wang, X.; Song, G.; Lou, T. Fabrication and characterization of nano-composite scaffold of PLLA/silane modified hydroxyapatite. *Med. Eng. Phys.* **2010**, *32* (4), 391−397.
(46) Xu, D.; Xu, Z.; Cheng, L.; Gao, X.; Sun, J.; Chen, L. Improvement of the mechanical properties and osteogenic activity of 3D-printed polylactic acid porous scaffolds by nano-hydroxyapatite and nano-magnesium oxide. *Heliyon* **2022**, *8* (6), No. e09748.
(47) Li, J.; Jiang, G.; Ding, F. The effect of pH on the polymer degradation and drug release from PLGA-mPEG microparticles. *J. Appl. Polym. Sci.* **2008**, *109* (1), 475−482.
(48) Wetteland, C. L.; de Jesus Sanchez, J.; Silken, C. A.; Nguyen, N.-Y. T.; Mahmood, O.; Liu, H. Dissociation of magnesium oxide and magnesium hydroxide nanoparticles in physiologically relevant fluids. *J. Nanopart. Res.* **2018**, *20*, 215.
(49) Fruhwirth, O.; Herzog, G.; Hollerer, I.; Rachetti, A. Dissolution and hydration kinetics of MgO. *Surf. Technol.* **1985**, *24* (3), 301−317.
(50) Zhang, N.; Lock, J.; Sallee, A.; Liu, H. Magnetic nanocomposite hydrogel for potential cartilage tissue engineering: synthesis, characterization, and cytocompatibility with bone marrow derived mesenchymal stem cells. *ACS Appl. Mater. Interfaces* **2015**, *7* (37), 20987−20998.
(51) Xu, C.; Uahengo, G.; Rudnicki, C.; Hung, C.; Huang, A.; Xu, Q.; Chen, Y.; Halaney, D. L.; Garay, J. E.; Mangolini, L.; et al. Nanocrystalline yttria-stabilized zirconia ceramics for cranial window applications. *ACS Appl. Bio Mater.* **2022**, *5* (6), 2664−2675.
(52) Xu, Q.; Zhang, Z.; Xiao, C.; He, C.; Chen, X. Injectable polypeptide hydrogel as biomimetic scaffolds with tunable bioactivity and controllable cell adhesion. *Biomacromolecules* **2017**, *18* (4), 1411−1418.
(53) Khorasani, M.; Mirzadeh, H.; Irani, S. Plasma surface modification of poly (l-lactic acid) and poly (lactic-co-glycolic acid) films for improvement of nerve cells adhesion. *Radiat. Phys. Chem.* **2008**, *77* (3), 280−287.
(54) Yang, L.; Gong, Z.; Lin, Y.; Chinthapenta, V.; Li, Q.; Webster, T. J.; Sheldon, B. W. Disordered topography mediates filopodial extension and morphology of cells on stiff materials. *Adv. Funct. Mater.* **2017**, *27* (38), 1702689.
(55) Yoshizawa, S.; Brown, A.; Barchowsky, A.; Sfeir, C. Magnesium ion stimulation of bone marrow stromal cells enhances osteogenic activity, simulating the effect of magnesium alloy degradation. *Acta Biomater.* **2014**, *10* (6), 2834−2842.


https://doi.org/10.1021/acsami.4c14712
*ACS Appl. Mater. Interfaces* 2025, 17, 3852−3865